ChemPubSoc Europe

DOI: 10.1002/cctc.201900777

CHEMCATCHEM Full Papers

Chemical Imaging of the Binder-Dependent Coke Formation in Zeolite-Based Catalyst Bodies During the Transalkylation of Aromatics

Suzanna P. Verkleij,[a] Gareth T. Whiting,*[a] Denise Pieper,[a] Sonia Parres Esclapez,[b] Shiwen Li,[b] Machteld M. Mertens,[b] Marcel Janssen,[b] Anton-Jan Bons,[b] Martijn Burgers,[b] and Bert M. Weckhuysen*[a]

The choice of binder material, added to a zeolite-based catalyst body, can significantly influence the catalyst performance during a reaction, i.e. its deactivation and selectivity. In this work the influence of the binder in catalyst extrudates on the formation of hydrocarbon deposits was explored during the transalkylation of toluene with 1,2,4-trimethylbenzene (1,2,4-TMB). Using in situ UV-vis micro-spectroscopy and ex situ confocal fluorescence microscopy approach, coke species were revealed to predominantly form on the rim of zeolite crystals within Al_2O_3-bound extrudates. It was found that this was due to Al migration between the zeolite crystals and the Al_2O_3-binder creating additional acid sites near the zeolite external surface. In contrast, minimal isomerization of 1,2,4-TMB in the SiO_2-bound extrudate allowed greater access to the zeolite internal pore network, creating a more homogeneous coke distribution throughout the zeolite crystals.

1. Introduction

Xylene is an important petrochemical compound that has many applications. *p*-Xylene is for example used in the production of terephthalic acid, which is a main component in polyethylene terephthalate (PET). Moreover, xylene (in particular, the isomers *p*-xylene and *o*-xylene) is used to produce plastics, polyester fibers, resins and plasticizers.[1–4] Xylene is mainly produced by steam cracking of heavy fractions and catalytic reforming of naphtha. Another possible route to make xylene is by the transalkylation of the less valuable molecules toluene and trimethylbenzene (TMB), which has attracted substantial research interests.[4–8] Simplified, the transalkylation of one mole of toluene and one mole of TMB forms two moles of xylene. However, the reaction of toluene and TMB on zeolites is rather complex, as multiple chemical reactions do occur.[9–12] Besides the transalkylation reaction, dealkylation, disproportionation and isomerization reactions can take place. In such instances, not only does the transalkylation pathway yield xylene, but also the disproportionation of two molecules of toluene or TMB can form xylene. Furthermore, the dealkylation of toluene forms benzene and the dealkylation of TMB results in the formation of xylene. Finally, the aromatic reactants can undergo isomerization reactions, for example 1,2,4-TMB can isomerize into the bulkier 1,2,3-TMB and 1,3,5-TMB.

For the performance of the zeolite catalyst during the transalkylation reaction, pore structure and acidity are two important factors. Firstly, the pores need to be large enough for the diffusion of the bulky TMB species. Previous studies have shown that 12-membered rings have a higher catalytic activity than 10-membered rings due to their enhanced diffusion capacity.[13–15] However, it was found that medium-pore zeolites, like ZSM-5, have a higher selectivity towards *p*-xylene.[16,17] Secondly, the reaction pathway taking place depends on the acid site strength. Previously, it has been shown that transalkylation and disproportionation mainly occur on strong acid sites, while isomerization can take place on weak acid sites.[18] Due to this isomerization, the selectivity towards *p*-xylene decreases.[19,20] Finally, it has been reported that the more bulky 1,3,5-TMB and 1,2,3-TMB, formed by the isomerization of 1,2,4-TMB, diffuse slower through medium-pore zeolite due to steric constrains and will mainly react at the surface of the zeolite.[21–23] However, direct visual evidence of this phenomena is still missing.

The importance of the zeolite acid site strength for the transalkylation reaction has mainly been investigated on pure zeolite powder. However, when zeolites are employed in an industrial reactor, they are usually combined with a binder

[a] S. P. Verkleij, Dr. G. T. Whiting, D. Pieper, Prof. Dr. B. M. Weckhuysen
Inorganic Chemistry and Catalysis
Debye Institute for Nanomaterials Science
Utrecht University
Universiteitsweg 99
Utrecht 3584 CG (The Netherlands)
E-mail: g.t.whiting@uu.nl
b.m.weckhuysen@uu.nl

[b] Dr. S. Parres Esclapez, S. Li, Dr. M. M. Mertens, Dr. M. Janssen, Dr. A.-J. Bons, Dr. M. Burgers
European Technology Centre
ExxonMobil Chemical Europe Inc.
Hermeslaan 2
Machelen 1831 (Belgium)

Supporting information for this article is available on the WWW under https://doi.org/10.1002/cctc.201900777

This publication is part of a Special Collection on "Advanced Microscopy and Spectroscopy for Catalysis". Please check the ChemCatChem homepage for more articles in the collection.

Table 1. BET surface areas[a] and pore volumes of the different samples under investigation[b], measured with Ar physisorption. Quantity of NH_3 per g of catalyst[c], measured with NH_3 TPD. Predicted surface areas, pore volumes and quantity of NH_3 are calculated with the ratio of the pure zeolite and the pure binder, and are shown between parentheses. The Na content in ppm of the different samples[d]. wt.% of coke after 1 h of transalkylation reaction at 450 °C on the catalyst extrudate[e], measured with thermogravimetric analysis (TGA).

	H-ZSM-5:binder [wt.%]	Binder	BET surface area [m^2/g][a]	Pore volume [cm^3/g][b]	NH_3 TPD [mmol/g][c]	Na content [ppm][d]	Coke[e] [wt.%]
H-ZSM-5	100:0	–	374	0.19	0.48	0	5
Al_2O_3	0:100	Al_2O_3	209	0.47	0.45	174	7
SiO_2	0:100	SiO_2	184	0.32	0.02	290	1
silicalite	100:0	–	413	0.19	0	13	1
20:80 SiO_2	20:80	SiO_2	221 (222)	0.28 (0.29)	0.12 (0.11)	174	2
20:80 Al_2O_3	20:80	Al_2O_3	241 (242)	0.49 (0.41)	0.46 (0.46)	83	7
sil20:80 Al_2O_3	20:80	Al_2O_3	261 (250)	0.52 (0.41)	0.43 (0.36)	203	4

material and shaped into catalyst bodies, such as extrudates. The shaping is done to improve the handling and attrition resistance, and to lower the pressure-drop (compared to a powder).[24] The addition of a binder material can have a large effect on the catalytic activity, as it can, for example, influence the overall acidity of the catalyst. [25,26] It has been shown that for shaped catalysts with an Al_2O_3 binder, Al migration can occur from the binder to the zeolite, creating extra acid sites.[27–30] It is however not known where such additional acid sites are located and how the additional acid sites affect the performance. Opposite to the Al_2O_3 binder, the addition of a SiO_2 binder can decrease the acidity of a zeolite catalyst. This was linked to the migration of silicon into the zeolite.[26,31,32] The results above show that the binder can have a significant influence (beneficial or detrimental) on the acidity of the catalyst and thus the catalytic performance.[24,25] Considering this and the limited application of high spatiotemporal chemical imaging techniques to study such intriguing features, it is vital to investigate the shaped catalyst body in more detail.

In this work, we investigate and visualize the influence of the binder material on the formation and location of coke molecules on the catalyst during the transalkylation of toluene and 1,2,4-TMB. Using *in situ* UV-vis micro-spectroscopy, we show there is a substantial difference in coke behavior between zeolite H-ZSM-5 containing mm-sized extrudates bound with either SiO_2 or Al_2O_3. Furthermore, the distinct location of the hydrocarbon species formed within each of the catalyst bodies, particularly coke, is imaged in 3-D with *ex situ* confocal fluorescence microscopy and the difference in product formation between the catalyst extrudates was investigated. As a proof of concept, we employ Al_2O_3-bound silicalite-based extrudates to demonstrate that the migration of Al in the Al_2O_3-bound extrudates are indeed responsible for the formation of additional acid sites.

2. Results and Discussion

2.1. Physicochemical Characterization of the Catalyst Materials

The different samples (zeolite-based extrudates and pure components) were characterized with scanning electron microscopy (SEM), Ar physisorption, NH_3 temperature programmed desorption (NH_3 TPD) and elemental analysis. The external surfaces of the cylindrical extrudates were imaged with SEM and the images are displayed in Figure S1 in the supporting information. The SEM images of the catalyst extrudates show that the zeolites are almost completely embedded in the extrudate and covered with the binder. This is the case for all extrudates, whatever the binder, and demonstrates that the different materials are comparable. Furthermore, the distribution of the H-ZSM-5 crystals within the extrudate was analyzed with SEM-EDX (Figure S2). The Si distribution within the extrudate is ascribed to the H-ZSM-5 crystals embedded in the Al_2O_3-binder, which is homogeneously distributed throughout the cross section.

The surface area and pore volume of the different studied samples were analyzed with Ar physisorption and the results are shown in Table 1. The results show that the BET surface area decreases when a binder material is added, due to the dilution of the zeolite in the sample (i.e. the BET surface area of 20:80 SiO_2, 221 m^2/g, is lower than that of H-ZSM-5 powder, 374 m^2/g). In contrast, the total pore volume increases with increasing binder content, due to the larger pores present in the binder. These trends in surface area and pore volume also apply to the silicalite samples. Furthermore, if the catalyst extrudates with the two binders are compared, it indicates that the pore volume of 20:80 Al_2O_3 (0.49 cm^3/g) or sil20:80 Al_2O_3 (0.52 cm^3/g) is higher than the pore volume of 20:80 SiO_2 (0.28 cm^3/g). The predicted surface areas and pore volumes are calculated using the ratio of pure components and are in good agreement with the experimental data.

NH_3 TPD was used to study the acidity of the different samples. The NH_3 TPD results in Table 1 (and Figure S3) show that the 20:80 Al_2O_3 extrudate contains more acid sites (0.46 mmol/g NH_3) than the 20:80 SiO_2 extrudate (0.12 mmol/g NH_3) due to the addition of the acid sites in the Al_2O_3 binder to those of the zeolite. As expected, the SiO_2 binder has no acid sites. The acidity values of the samples are similar to the expected values, except for the sil20:80 Al_2O_3 extrudate that has a higher quantity of acid sites than expected. Furthermore, elemental analysis was used to determine the purity of the samples. As shown in Table 1, the H-ZSM-5 crystals do not contain any Na impurities. However, the binders themselves do

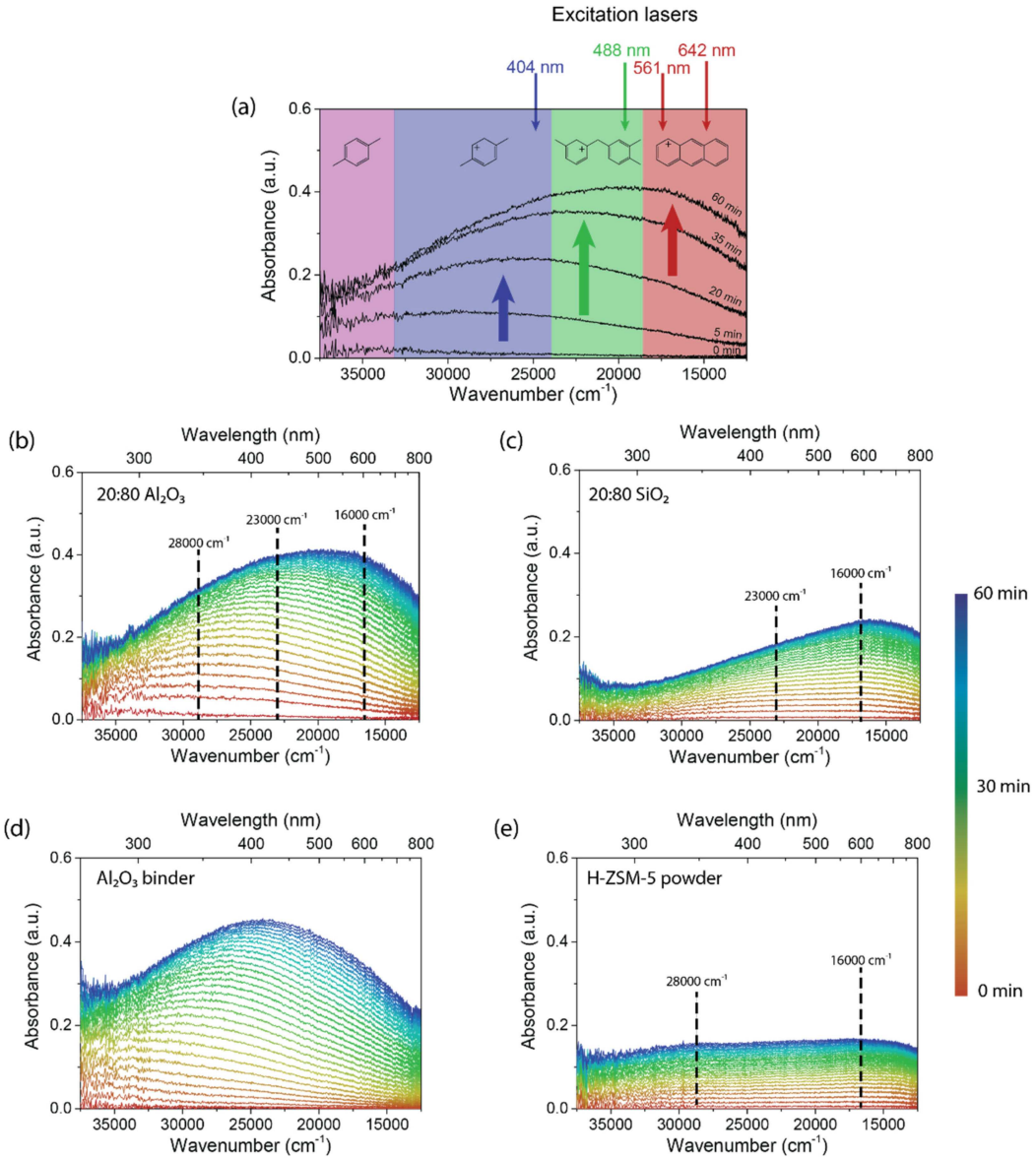

Figure 1. (a) Schematic of different regions that increase in absorption in the diffuse reflectance UV-vis spectra during the reaction of toluene and 1,2,4-TMB. In the different spectral regions, an example of the type of molecule that absorbs the light is presented. The laser line wavelengths used to excite such molecules within confocal fluorescent microscopy are also highlighted. Time resolved *in situ* diffuse reflectance UV-vis spectra during the transalkylation of toluene and 1,2,4-TMB at 450 °C, over (b) 20:80 Al_2O_3, (c) 20:80 SiO_2, (d) Al_2O_3 binder and (e) H-ZSM-5 powder for 1 h. The dashed lines indicate an absorption region in the diffuse reflectance UV-vis spectra.

contain a small amount of Na ions, which introduces a small amount of Na atoms into the extrudate samples.

2.2. Coke Formation During Transalkylation at 450 °C

In situ diffuse reflectance UV-vis micro-spectroscopy was used to follow the coke formation during the transalkylation of toluene and 1,2,4-trimethylbenzene (1,2,4-TMB) on the extrudates. The (charged) aromatic species formed during reaction are known to absorb light due to their π–π^* transitions, leading to specific absorption regions in the UV-vis spectra (Figure 1a). Absorption in the region above 33000 cm^{-1} (< 300 nm) is attributed to the reactants and formation of products. During the reaction, in the region around 28000 cm^{-1} (350 nm) and around 23000 cm^{-1} (430 nm), absorption increases due to the formation of charged alkylated aromatics (which are the reaction intermediates), as shown in Figure 1a. The smaller the wavenumber, the more conjugated the molecules are.[33] In the region around 16000 cm^{-1} (625 nm) absorption is due to the formation of poly-aromatic molecules that block the pores of the zeolite and hence cause deactivation.[3,34,35]

Figure 1b and c show the time resolved *in situ* diffuse reflectance UV-vis spectra during the transalkylation reaction of toluene and 1,2,4-TMB on 20:80 Al_2O_3 and 20:80 SiO_2 extrudates, respectively. In the UV-vis diffuse reflectance spectra

of 20:80 SiO_2, the tail-end of an absorption band at around 40000 cm^{-1} (250 nm) is visible, due to the absorption of the reactants and products. During reaction, in the region around 23000 cm^{-1} (430 nm) and around 16000 cm^{-1} (625 nm), the absorption increases in intensity, with these regions assigned to alkylated benzene carbocations, charged diphenylmethane (reaction intermediates) and large poly-aromatic molecules, respectively. For the 20:80 Al_2O_3 extrudates, an extra absorption band is formed in the region around 28000 cm^{-1} (350 nm) in comparison to 20:80 SiO_2, which can be assigned to charged methylated benzene carbocations. Furthermore, in the 20:80 Al_2O_3 spectra, the absorption around 23000 cm^{-1} (430 nm) and 16000 cm^{-1} (625 nm) are significantly higher in intensity than in the 20:80 SiO_2 spectra, indicating that the Al_2O_3 extrudates form a higher concentration of more large conjugated species. Thermogravimetric analysis (TGA) (Table 1) was used to measure the amount of residue in the samples and to verify the *in situ* UV-vis results. The weight % of residue in 20:80 Al_2O_3 (7 wt.%) is higher than that of 20:80 SiO_2 (2 wt.%), which corresponds well with the diffuse reflectance UV-vis spectra, showing that more poly-aromatic species are formed for the 20:80 Al_2O_3 sample.

The differences between the diffuse reflectance UV-vis spectra of 20:80 Al_2O_3 and 20:80 SiO_2 extrudates can be largely explained by the presence of Al_2O_3 binder. The *in situ* diffuse reflectance UV-vis spectra of pure Al_2O_3 (Figure 1d) displays a large absorption around 28000 cm^{-1} (350 nm), which becomes more intense and shifts to lower wavenumbers due to the formation of charged alkylated benzenes. The weak acid sites present in the Al_2O_3 binder can bind with the toluene and 1,2,4-TMB, and form these charged alkylated aromatics. However, the catalytic data (vide infra) show that pure Al_2O_3 extrudates do not form any products. Although the difference in diffuse reflectance UV-vis spectra between 20:80 Al_2O_3 and 20:80 SiO_2 can largely be explained by the absorption band formed on the Al_2O_3 binder, it does not explain the entire difference. For the ZSM-5-bound catalyst extrudates, the amount of poly-aromatic compounds formed is higher than can be expected from the combination of the H-ZSM-5 spectra (Figure 1e) and the binders alone (Al_2O_3 binder in Figure 1d and SiO_2 binder in Figure S4). Previously, it has been shown that species (such as Si and/or Al) can migrate from the binder to the zeolite and vice versa and for extrudates with Al_2O_3 binder, the migration of Al creates extra acid sites within the extrudate.[27–30]

In correlation with *in situ* diffuse reflectance UV-vis spectroscopy results, whereby the formation of poly-aromatic coke molecules was monitored, 3-D confocal fluorescence microscopy has been used to chemically image the location of such species within catalyst extrudates. The samples were illuminated with four lasers of different wavelengths, namely, 404 nm, 488 nm, 561 nm and 642 nm, as shown in Figure 1a. Certain molecules are excited by a laser with a wavelength in the absorption band of these molecules and can, subsequently, fluoresce. In the 3-D chemical image, the fluorescent molecules have a different color, namely: blue for 404 nm laser excitation; green for the 488 nm laser; and red for both the 561 nm and 642 nm laser.

Figure 2 shows the *ex situ* 3-D confocal fluorescence microscopy images of 20:80 Al_2O_3, 20:80 SiO_2 and H-ZSM-5 imaged after 1 h of reaction. In all three samples, only the molecules present in/on the zeolite crystals are displaying fluorescence, whereas the binders themselves do not have any fluorescence, as displayed in Figure S5. Molecules within the zeolite crystals in the 20:80 SiO_2 extrudate (Figure 2b) exhibit fluorescence when excited with all lasers, except 404 nm. Comparing the 20:80 SiO_2 with the 20:80 Al_2O_3 (Figure 2a) shows that the molecules inside the Al_2O_3-bound extrudate fluoresce when excited at longer wavelengths. This is due to larger conjugated poly-aromatic molecules inside the extrudate, as observed with diffuse reflectance UV-vis spectroscopy (Figure 1b) and TGA (Table 1). Compared to the binder-bound extrudates, the H-ZSM-5 powder displays fluorescence when excited at shorter wavelengths, confirming the less conjugated nature of the coke species, as observed by diffuse reflectance UV-vis spectroscopy.

Not only the type of coke molecules is different for the 20:80 SiO_2 and 20:80 Al_2O_3 extrudates, but also the location of the coke molecules in the zeolite crystals. Two different types of coking profiles in the embedded zeolite crystals can be distinguished: type A, has mainly fluorescence (coke) at the edge of the zeolite crystals, with a thickness of <1 μm; and type B, where zeolite crystals are completely fluorescent (coked) throughout. To distinguish between Type A and Type B coke characteristics, first the center of the zeolite is identified by scrolling through the 3-D image. To have a Type A coke profile, the center must clearly have a lower fluorescence intensity then the edge, otherwise it is marked as a Type B coke profile. The right column in Figure 2 shows the ratio of type A to type B zeolite crystals displayed on average in each extrudate. It is clear that the SiO_2 binder does not influence the location of the fluorescent coke molecules, as the zeolites within 20:80 SiO_2 mainly display a type B coking profile, which is similar to the H-ZSM-5 powder. In contrast to the SiO_2 extrudate, the 20:80 Al_2O_3 extrudate displays a substantially higher quantity of type A than type B crystals, when compared to the H-ZSM-5 powder. Previously, it has been shown that Al migration between the binder and the zeolite can occur for catalysts shaped with an Al_2O_3 binder, creating extra acid sites.[27–30] These acid sites could contribute to the unusual spatial distribution of the coke species on the edge region of the ZSM-5 crystals.

2.3. Linking Binder-Effects to the Spatial Coke Distribution

To investigate whether the creation of additional acid sites can contribute to the specific location of coke species, extrudates containing 20 wt.% silicalite crystals bound with 80 wt.% Al_2O_3 (sil20:80 Al_2O_3) were prepared and evaluated. Silicalite crystals do not contain aluminum and consequently have no acid sites. However, if Al migrates from the Al_2O_3 binder to the silicalite crystals, acid sites can be created.[27–30] The *in situ* diffuse reflectance UV-vis spectra of the sil20:80 Al_2O_3 extrudate (Figure 3) display the formation of several absorption bands during the transalkylation reaction. The absorption in the

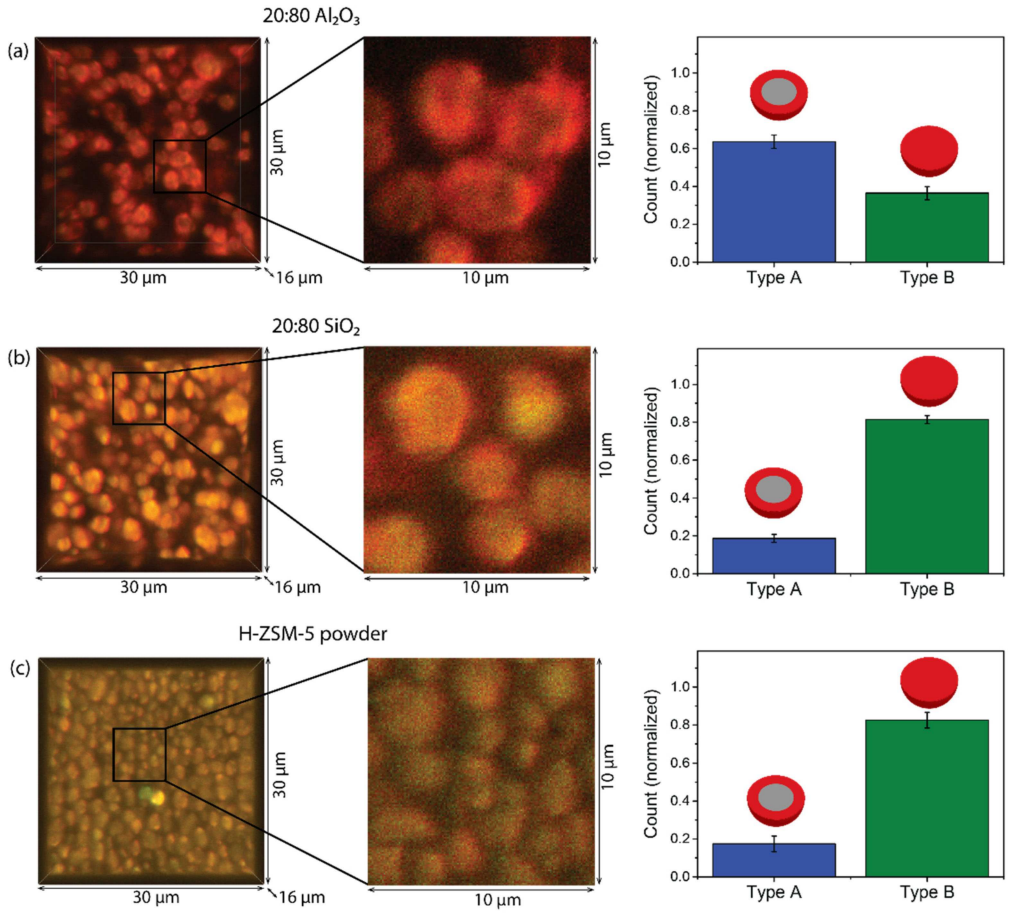

Figure 2. *Ex situ* 3-D confocal fluorescence microscopy images taken after 1 h of transalkylation of toluene and 1,2,4-TMB at 450 °C, for (a) 20:80 Al_2O_3, (b) 20:80 SiO_2 and (c) H-ZSM-5 powder. Excitation with 404 nm, 488 nm, 562 nm and 642 nm laser causes respectively the blue, green and red (both 562 and 642 nm laser) fluorescence. For all samples an enlargement of the marked area is shown in the center panel. On the right side of the image the ratio of different types of coke formation in the corresponding sample is plotted. Type A has mainly coke molecules at the rim of the zeolite crystals and type B has coke molecules throughout the crystal.

regions around 28000 cm^{-1} (350 nm) and 23000 cm^{-1} (430 nm) can be assigned to charged alkylated aromatics.[35] The large absorption band around 28000 cm^{-1} (350 nm) can also be found in the UV-vis diffuse reflectance spectra of the Al_2O_3 binder (Figure 1d). Additionally, absorption around 16000 cm^{-1} (625 nm) appears due to the formation of large poly-aromatic molecules. The latter molecules cannot be formed by either of the two separate components (Al_2O_3 binder in Figure 1d and silicalite powder in Figure 3b). This confirms that acid sites are created upon mixing/binding of the individual components and can indeed participate in this reaction.

Whether or not the location of these acid sites can influence the spatial distribution of coke species was confirmed using *ex situ* 3-D confocal fluorescence microscopy on the silicalite-based extrudates after reaction. As the silicalite containing extrudates have less acid sites and consequently contain a lower concentration of coke molecules, the CFM images were measured at a higher laser power for visibility. The 3-D chemical image of sil20:80 Al_2O_3, in Figure 3c, again indicates the formation of poly-aromatic species, corroborating the diffuse reflectance UV-vis spectra (Figure 3a). As the fluorescent poly-aromatic coke molecules are located only on the previously inert silicalite crystals (Figure S5), the creation of additional acid sites is unequivocal. Remarkably, the sil20:80 Al_2O_3 sample also displays both type A and type B coking profiles, even though it is more difficult to distinguish between type A and type B coking profiles than for the ZSM-5 containing extrudates, due to the lower fluorescence intensity in the silicalite containing extrudates. In particular, the presence of type A coking, indicates that indeed, acid sites created at the zeolite crystal 'rim' do contribute to corresponding 'rim' formation of coke species.

The creation of extra acid sites influences the acidic properties of the catalyst and can consequently influence the transalkylation reaction. The differences in catalyst performance during the reaction were therefore tested in a fixed bed reactor. Figure 4 shows the total conversion, *m*/*p*-xylene yield and 1,3,5-TMB yield per g of catalyst, as a function of time on stream. Comparing the total conversion for the Al_2O_3-bound catalyst extrudate with the SiO_2-bound catalyst extrudate shows a two-fold increase for the Al_2O_3-bound extrudate, even though both extrudates contain 20 wt.% of H-ZSM-5 zeolite crystals. This

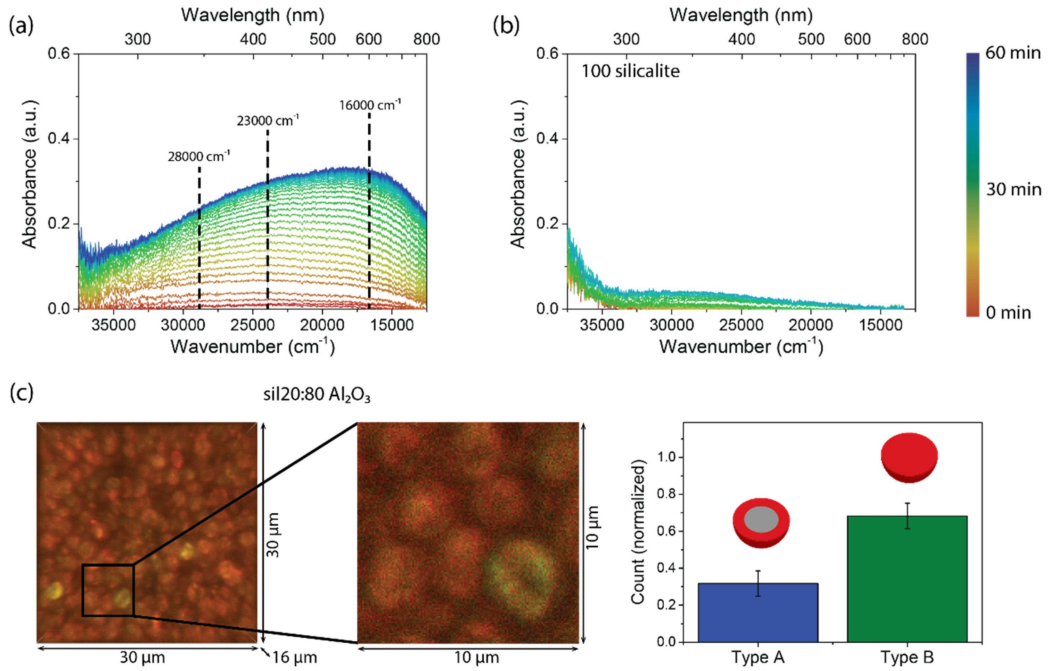

Figure 3. Time resolved *in situ* diffuse reflectance UV-vis spectra during the transalkylation of toluene and 1,2,4-TMB at 450 °C, over (a) sil20:80 Al_2O_3 and (b) 100 silicalite for 1 h. The dashed lines indicate an absorption region in the diffuse reflectance UV-vis spectra. (c) *Ex situ* 3-D confocal fluorescence microscopy images taken after 1 h of transalkylation of toluene and 1,2,4-TMB at 450 °C, for sil20:80 Al_2O_3. Excitation with 404 nm, 488 nm, 562 nm and 642 nm laser causes the blue, green and red (both 562 and 642 nm laser) fluorescence, respectively. An enlargement of the marked area is shown in the center of the image. The fluorescence images were measured with a higher laser power than the previous images. On the right side of the image the ratio of different types of coke formation in the corresponding sample is plotted. Type A has mainly coke molecules at the rim of the zeolite crystals; and type B has coke molecules throughout the crystal.

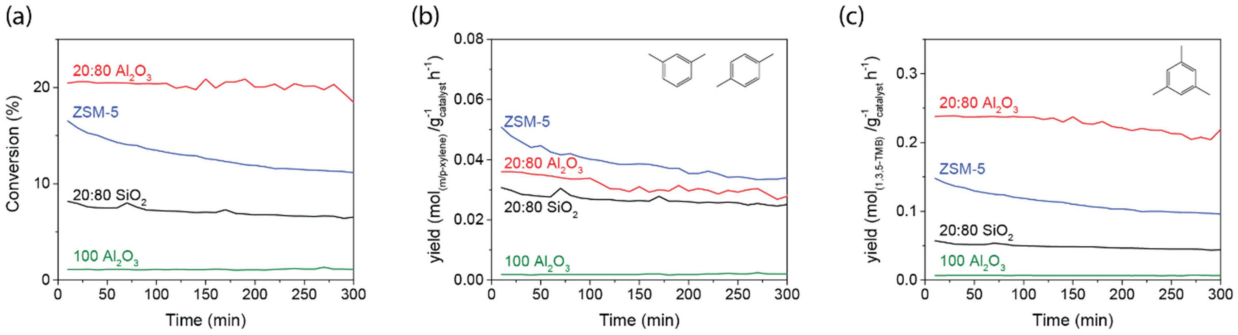

Figure 4. (a) Total feed conversion, (b) *m/p*-xylene and (c) 1,3,5-TMB yield as a function of time on stream, during the transalkylation reaction of toluene and 1,2,4-TMB over 20:80 Al_2O_3 (red), 20:80 SiO_2 (black), ZSM-5 (blue) and 100 Al_2O_3 (green) at 450 °C and 2 h^{-1} WHSV. The results are normalized per g of catalyst.

increase in conversion is not due to the Al_2O_3 binder itself as the 100 Al_2O_3 extrudate is unreactive and therefore must be due to a binder effect in the 20:80 Al_2O_3 extrudate, for example the increase in acid sites at the surface of the zeolite crystals within the extrudates. These results are consistent with the UV-vis results, as the formation rate for the absorption bands is higher for the 20:80 Al_2O_3 catalyst extrudate than for the 20:80 SiO_2 catalyst extrudate, indicating a higher conversion.

Furthermore, the yields of both *m/p* xylene and 1,3,5-TMB can be compared for the 20:80 Al_2O_3 and 20:80 SiO_2 catalyst extrudate. The xylene yield is similar for both the extrudate samples, which is expected as both samples contain 20 wt.% of H-ZSM-5 crystals. However, the 1,3,5-TMB yield is higher for the 20:80 Al_2O_3 extrudate compared to the 20:80 SiO_2 extrudate. Taking into account that confocal fluorescence microscopy showed that the 20:80 Al_2O_3 catalyst extrudate forms coke on the rim of the zeolite crystals embedded in the extrudate, we suggest that extra acid sites are created between the zeolite and the binder. These extra acid sites can isomerize the 1,2,4-TMB into 1,3,5-TMB. Dumitriu et al.[18] showed that trimethylbenzene can isomerize on weaker acid sites, whereas the transalkylation and disproportionation occur on stronger acid sites. The 1,3,5-TMB, which is isomerized at the edge of the zeolite, is larger and diffuses slower through the zeolite pores,

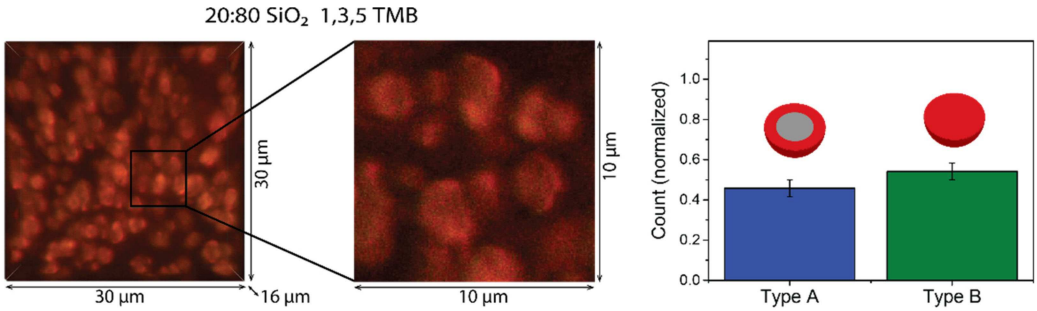

Figure 5. *Ex situ* 3-D confocal fluorescence microscopy images taken of 20:80 SiO_2 extrudate after 1 h of reaction with 1,3,5-TMB. Excitation with 404 nm, 488 nm, 562 nm and 642 nm laser causes respectively the blue, green and red (both 562 and 642 nm laser) fluorescence. For all samples, an enlargement of the marked area is shown in the center panel. On the right side of the image the ratio of different types of coke formation in the corresponding sample is plotted. Type A has mainly coke molecules at the rim of the zeolite crystals; and type B has coke molecules throughout the crystal.

causing coke to form on the rim of the ZSM-5 zeolite. As the conversion includes the formation of TMB isomers, the increased conversion for the 20:80 Al_2O_3 extrudates is due to the increased formation of 1,3,5-TMB.

To explore if the type A coking of the zeolite crystals is indeed caused by the reaction of sterically hindered 1,3,5-TMB at the zeolite external surface, the 20:80 SiO_2 extrudate was reacted with only 1,3,5-TMB under the same reaction conditions as the previous toluene and 1,2,4-TMB reaction. Figure 5 shows the fluorescence microscopy images of the extrudate after reaction with 1,3,5-TMB and the corresponding *in situ* diffuse reflectance UV-vis spectra are shown in Figure S6. The results demonstrate there is a 2.5 times increase in type A coke formation compared to the reaction with toluene and 1,2,4-TMB on 20:80 SiO_2 (Figure 2b). This confirms that 1,3,5-TMB reacts at the outside of the zeolite crystals, and provides the first direct visual confirmation that a rim of coke species can be formed near the external surface of zeolite crystals in industrial-grade catalysts.

The consequence of the creation of extra acid sites in Al_2O_3-bound extrudates is that more coke species are formed at the edge of the zeolite crystals. Furthermore, the extra acid sites also dramatically influence the selectivity of the catalyst, particularly yielding more isomerization products. This should be considered when selecting specific binders for alkylation-type reactions.

3. Conclusions

Using a combination of *in situ* diffuse reflectance UV-vis micro-spectroscopy and *ex situ* confocal fluorescence microscopy, we demonstrate that the choice of the binder material has a large effect on the deactivation of catalyst extrudates during the transalkylation of toluene with 1,2,4-trimethylbenzene. The deactivation process during the transalkylation reaction was investigated for millimeter-sized zeolite H-ZSM-5-containing catalyst extrudates with either SiO_2 or Al_2O_3 as binder material. UV-vis micro-spectroscopy combined with TGA, showed that the catalyst extrudate with 20:80 Al_2O_3 binder forms larger poly-aromatic species than the catalyst extrudate with SiO_2 binder. The difference cannot be explained by the two separate components, and must be due to binder effects occurring upon the combination of the components. Furthermore, using complementary confocal fluorescence microscopy, it was demonstrated that in the catalyst extrudate containing SiO_2 binder, the coke is formed predominantly throughout the zeolite crystals, similar to the zeolite H-ZSM-5 without binder. In the Al_2O_3 extrudate, however, the coke is mainly formed on the rim of the zeolite crystals. Both discrepancies between the two different extrudates (more coke formation and coke at the rim of the zeolite for the Al_2O_3-bound extrudate) were explained by the creation of extra acid sites on the zeolite/binder interface. The migration of species was confirmed by performing the transalkylation reaction on extrudates containing silicalite crystals (i.e., in the absence of aluminum) bound with Al_2O_3. It was shown that these catalyst extrudates contain acid sites created by Al migration and form poly-aromatic species during reaction, that were not observed for the corresponding individual components of the extrudate. These acid sites enhance 1,2,4-TMB isomerization into bulkier 1,3,5-TMB and 1,2,3-TMB. The 1,3,5-TMB reacts mainly at the zeolite external surface to form coke, which was confirmed by the reaction of 1,3,5-TMB on the SiO_2-bound catalyst extrudate. Such visual confirmation of both binder effects in zeolite catalyst bodies could shed light into how to limit or enhance binder effects by catalyst design, in order to prolong catalyst lifetime, or to minimize the formation of side products during a catalytic reaction.

Experimental Section

H-ZSM-5 extrudates bound with Al_2O_3 or SiO_2 as binder material were used for the transalkylation reaction of toluene and 1,2,4-trimethylbenzene (1,2,4-TMB). The SiO_2- or Al_2O_3-bound extrudates were prepared by mixing zeolite ZSM-5 crystals with H_2O, extrusion aid and binder, according to patent US6,039,864.[36] The zeolite H-ZSM-5 crystals had a Si/Al ratio of 32 and an average crystal size of 3 µm. For the SiO_2-bound extrudates, SiO_2 gel (AEROSIL 300) and silica sol (NALCOAG 1034A) were used as binder and, for the Al_2O_3 bound extrudates, pseudoboehmite alumina (Versal 300) was used as binder. The prepared mixture was extruded into 1 mm extrudates, dried overnight at 130 °C and calcined at 500 °C for

18 h. Ion-exchange was performed by suspending the extrudates in a 1 M ammonium nitrate solution for 4 h, followed by washing and drying and a final calcination at 500 °C for 18 h.

The formed extrudates contained 20 wt.% H-ZSM-5 and 80 wt.% Al_2O_3 or SiO_2 binder. The small zeolite weight ratio of 20:80 wt.% was chosen, so as to observe the effects of the binder more clearly. The different samples were named as follows: *A:B* binder, in which "*A*" corresponds to the wt.% H-ZSM-5 content and "*B*" corresponds to the wt.% binder, for example, '20:80 SiO_2' is an 80 wt.% SiO_2 bound extrudate containing 20 wt.% H-ZSM-5 crystals. Furthermore, reference extrudates, containing only binder, and zeolite H-ZSM-5 powder were used. Additionally, silicalite extrudates were used and the extrudates containing 20 wt.% silicalite and 80 wt.% Al_2O_3 binder were named, 'sil20:80 Al_2O_3'.

The different catalysts were characterized with scanning electron microscopy (SEM), Ar physisorption, NH_3 temperature programmed desorption (NH_3 TPD) and elemental analysis. SEM analysis was conducted by attaching a whole extrudate to a SEM stub and coated with Pd/Pt in a Cressington 208HR sputter coater. The surface of the extrudate was imaged on a JEOL JSM-6340F Field Emission Gun Scanning Electron Microscope (FEG-SEM) operated at 5 kV using secondary electrons. The surface area and pore volume of the samples were measured with Ar physisorption. First the extrudates were dried under vacuum at 300 °C overnight. All samples were measured with a Micromeritics TriStar 3000 at 77 K. The surface area was calculated with the Brunauer-Emmett-Teller (BET) method and the t-plot method was used to determine the pore volume. NH_3 TPD was used to measure the acidity of the samples and the measurements were performed on a Mettler Toledo TGA/SDTA 851. Prior to NH_3 TPD, the samples were dried at 550 °C under He flow with a heating rate of 10 °C/min for 15 min. Subsequently, the samples were exposed to 12 pulses of 10% NH_3 in He at 100 °C. By applying a temperature ramp to 550 °C with 5 °C/min under He flow, desorption data have been collected. The amount of desorbed ammonia was monitored with a thermal conductivity detector (TCD). Finally, elemental analysis was done on a Varian Vista MPX Inductively Coupled Plasma Optical Emission Spectrometer using multi-element standards provided by Merck and Alfa Aesar. Before analysis, around 200 mg of the sample was dissolved in a mixture of acids (30% HCl, 3 mL; 65% HNO_3, 1 mL; 40% HF, 2 mL) for 4–5 h (the first hour with sonication) and then further diluted to 100 mL milli-Q water.

The catalytic tests were performed in a fixed-bed reactor with an internal diameter of 10 mm, which was operated in up flow mode. The reactor was loaded with approximately 2 g of crushed and sieved catalyst with a particle size of 0.2 - 0.4 mm. Prior to the catalytic reaction, the catalyst was activated under N_2 flow at 450 °C for 1 hour. The reactants were delivered via an ISCO pump with a 1:1 molar ratio of toluene:1,2,4-TMB and a WHSV of 2 h^{-1}. The products were analyzed with a GC equipped with DBWAX column. The conversion and product yields were calculated from the GC results, assuming that the response factor for all the reactants and products is 1 and the results were calculated per gram of catalyst.

Deactivation of the different samples was followed with *in situ* diffuse reflectance UV-vis micro-spectroscopy under similar conditions as the catalytic tests. The reaction was performed in a TS1500 V Linkam Scientific Instruments cell coupled with a TMS94 temperature controller and a PSU1500 unit from Linkam Scientific Instruments. This is a small heating plate on which the extrudates are placed. An additional calcination was performed before reaction, by heating the samples to 500 °C with 10 °C/min under a 1:1 flow ratio of N_2 and O_2 for 1 h. The transalkylation reaction was performed at 450 °C for 1 h. For this reaction, toluene and 1,2,4-TMB were put in separate saturators and N_2 was bubbled through the separate saturators, to reach a 1:1 molar ratio and when 1,3,5-TMB was reacted, an N_2 flow of 16.1 ml/min was used. The reactants were evaporated by bubbling N_2 through a saturator and subsequently flown over the extrudates. Diffuse reflectance UV-vis micro-spectroscopy measurements were performed on a CRAIC 20/30 PV™ micro-spectrophotometer equipped with a 15x 0.28 NA reflective lens and a 30 W halogen lamp. During reaction, the diffuse reflectance spectra were collected from a region (82 × 82 μm) on top of the extrudate external surface and were always taken on the first extrudate that the flow of reactants reaches. The spectra were recorded every 10 s for 1 h.

After 1 h of reaction, the coke formation on the samples was imaged with *ex situ* confocal fluorescence microscopy using a Nikon Eclipse 90i instrument equipped with a 100×0.73 NA dry objective. The sample was excited with four different laser lines; 404 nm, 488 nm, 561 nm and 642 nm and the emission was detected with an A1-DU4 4 detector unit in the range of 425–475 nm, 500–550 nm, 570–620 nm and 662–737 nm, respectively. Only the in-focus light is collected by the detector due to a pinhole. By making 2-D microscopy images at different focal depths, a 3-D chemical image is composed. To determine the different types of coking of the zeolite crystals in each of the 3-D images, two spots on three different extrudates were manually counted. Furthermore, after the reaction, the hydrocarbon deposits inside the extrudate were characterized with thermogravimetric analysis (TGA). The samples were heated to 700 °C with 5 °C/min under 10 ml/min O_2 on a PerkinElmer pyris 1 TGA instrument.

Acknowledgements

We thank Marjan Versluijs-Helder (Utrecht University, UU) for all the SEM and TGA measurements and Serguei Matveev (UU) for the SEM-EDX measurements. This work was financially supported by ExxonMobil. G.T.W. acknowledges a NWO personal 'Veni' grant (722.015.003).

Conflict of Interest

The authors declare no conflict of interest.

Keywords: Fluorescence spectroscopy · UV/vis spectroscopy · zeolites · transalkylation · in-situ microscopy

[1] W. Vermeiren, J.-P. Gilson, *Top. Catal.* **2009**, *52*, 1131–1161.
[2] J. M. Serra, E. Guillon, A. Corma, *J. Catal.* **2005**, *232*, 342–354.
[3] S. Al-Khattaf, S. A. Ali, A. M. Aitani, N. Žilková, D. Kubička, J. Čejka, *Catal. Rev. Sci. Eng.* **2014**, *56*, 333–402.
[4] R. Thakur, S. Barman, R. K. Gupta, *Chem. Eng. Commun.* **2017**, *204*, 254–264.
[5] J. Hanika, Q. Smejkal, A. Krejci, J. Kolena, D. Kubicka, *Petr. Coal.* **2003**, *45*, 78–82.
[6] S. A. Ali, K. E. Ogunronbi, S. S. Al-Khattaf, *Chem. Eng. Res. Des.* **2013**, *91*, 2601–2616.
[7] A. Krejčí, S. Al-Khattaf, M. A. Ali, M. Bejblová, J. Čejka, *Appl. Catal. A* **2010**, *377*, 99–106.
[8] S. H. Cha, S. B. Hong, *J. Catal.* **2018**, *357*, 1–11.
[9] J. Čejka, B. Wichterlová, *Catal. Rev.* **2002**, *44*, 375–421.
[10] S. Al-Khattaf, M. N. Akhtar, T. Odedairo, A. Aitani, N. M. Tukur, M. Kubů, Z. Musilová-Pavlačková, J. Čejka, *Appl. Catal. A* **2011**, *394*, 176–190.
[11] S. A. Ali, A. M. Aitani, C. Ercan, Y. Wang, S. Al-Khattaf, *Chem. Eng. Res. Des.* **2011**, *89*, 2125–2135.

[12] J. Toda, A. Corma, G. Sastre, *J. Phys. Chem. C.* **2016**, *120*, 16668–16680.
[13] S. Al-Khattaf, N. M. Tukur, A. Al-Amer, *Ind. Eng. Chem. Res.* **2007**, *46*, 4459–4467.
[14] I. Wang, T. C. Tsai, S. T. Huang, *Ind. Eng. Chem. Res.* **1990**, *29*, 2005–2012.
[15] S. M. Waziri, A. M. Aitani, S. Al-Khattaf, *Ind. Eng. Chem. Res.* **2010**, *49*, 6376–6387.
[16] Y. Li, H. Wang, M. Dong, J. Li, Z. Qin, J. Wang, W. Fan, *RSC Adv.* **2015**, *5*, 66301–66310.
[17] F. J. Llopis, G. Sastre, A. Corma, *J. Catal.* **2004**, *227*, 227–241.
[18] E. Dumitriu, C. Guimon, V. Hulea, D. Lutic, I. Fechete, *Appl. Catal. A* **2002**, *237*, 211–221.
[19] S. Zheng, A. Jentys, J. A. Lercher, *J. Catal.* **2006**, *241*, 304–311.
[20] J. Čejka, B. Wichterlová, *Catal. Rev.* **2002**, *44*, 375–421.
[21] S. H. Park, H. K. Rhee, *Catal. Today.* **2000**, *63*, 267–273.
[22] H. P. Röger, K. P. Möller, C. T. O'Connor, *Microporous Mater.* **1997**, *8*, 151–157.
[23] N. M. Tukur, S. Al-Khattaf, *Energy and Fuels.* **2007**, *21*, 2499–2508.
[24] S. Mitchell, N.-L. Michels, J. Pérez-Ramírez, *Chem. Soc. Rev.* **2013**, *42*, 6094–6112.
[25] J. S. J. Hargreaves, A. L. Munnoch, *Catal. Sci. Technol.* **2013**, *3*, 1165–1171.
[26] N.-L. Michels, S. Mitchell, J. Pérez-Ramírez, *ACS Catal.* **2014**, *4*, 2409–2417.
[27] G. T. Whiting, F. Meirer, M. M. Mertens, A.-J. Bons, B. M. Weiss, P. A. Stevens, E. de Smit, B. M. Weckhuysen, *ChemCatChem.* **2015**, *7*, 1312–1321.
[28] Y. Zhang, Y. Zhou, A. Qiu, Y. Wang, Y. Xu, P. Wu, *Ind. Eng. Chem. Res.* **2006**, *45*, 2213–2219.
[29] M. W. Kasture, P. S. Niphadkar, V. V. Bokade, P. N. Joshi, *Catal. Commun.* **2007**, *8*, 1003–1008.
[30] A. Martin, H. Berndt, U. Lohse, U. Wolf, *J. Chem. Soc. Faraday Trans.* **1993**, *89*, 1277–1282.
[31] P. Gélin, T. Des Courières, *Appl. Catal.* **1991**, *72*, 179–192.
[32] P. Gelin, C. Gueguen, *Appl. Catal.* **1988**, *38*, 225–233.
[33] K. Hemelsoet, Q. Qian, T. De Meyer, K. De Wispelaere, B. De Sterck, B. M. Weckhuysen, M. Waroquier, V. Van Speybroeck, *Chem. Eur. J.* **2013**, *19*, 16595–16606.
[34] M. Guisnet, P. Magnoux, *Appl. Catal. A* **2001**, *212*, 83–96.
[35] F. Chen, G. Coudurier, C. Naccache, *Stud. Surf. Sci. Catal.* **1989**, *49*, 1387–1396.
[36] G. D. Mohr, J. P. Verduijn, Hydrocarbon Conversion Process Using Zeolite Bound Zeolite Catalyst, US6,039,864A, **2000**.

Manuscript received: April 28, 2019
Revised manuscript received: August 10, 2019
Accepted manuscript online: August 14, 2019
Version of record online: September 4, 2019